Science of Remote Sensing 11 (2025) 100237

Contents lists available at ScienceDirect

Science of Remote Sensing

journal homepage: www.sciencedirect.com/journal/science-of-remote-sensing

High-resolution mapping of orchard distribution across Italy

Francesco Lodato [a,b], Ryan Jayne [c], Marco Santonico [a], Maurizio Pollino [d], Flavio Bellino [e], Laura De Gara [f], Bruno Basso [c,g,*]

[a] Department of Science and Technology for Sustainable Development and One Health, Research Unit of Electronics for Sensor Systems, Università Campus Bio-Medico di Roma, via Álvaro del Portillo, Rome, 00128, Italy
[b] Department of Biology, University of Naples Federico II, Naples, 80138, Italy
[c] Dept. Earth and Environmental Sciences and W.K. Kellogg Biological Station, Michigan State University, 288 Farm Lane, East Lansing, MI, 48823, USA
[d] ENEA - Italian National Agency for new technologies, energy and sustainable economic development, Casaccia Research Centre, Via Anguillarese 310, Rome, 00123, Italy
[e] TIMAC AGRO Italia, SP13, Ca' Nova, CR, 26010, Italy
[f] Unit of Food Science and Human Nutrition, Università Campus Bio-Medico di Roma, via Álvaro del Portillo, Rome, 00128, Italy
[g] W.K. Kellogg Biological Station, Michigan State University, 288 Farm Lane, East Lansing, MI, 48823, USA

A R T I C L E I N F O

Keywords:
Large scale crop detection
Orchard classification
LULC
Machine

A B S T R A C T

Accurate large-scale orchard mapping is crucial for agricultural development and sustainable resource management. However, achieving this on a broad scale presents significant challenges, primarily due to the high costs and complexities associated with in-situ sampling and georeferencing. Remote sensing is valuable for accurate mapping of orchard, yet certain areas remain a challenge due to their heterogeneous spatial and temporal nature, influenced by climate, soil, local management practices and other phenomena, that make each orchard unique, especially in highly fragmented landscapes. In this study, we propose a method for large-scale crop mapping at high spatial resolution, using Italy as a case study. We utilized a dense spectro-temporal cube of Sentinel-2 and Sentinel-1 images with pyramidal-based sampling, employing available georeferenced polygons. A probabilistic XGB classifier was applied, followed by a Bayesian approach using prior data from the national statistical system to calibrate the final classification probabilities.

The final scope of this study is to enhance the specificity of certain subclasses within Corine Land Cover class 2 in Italy, with a particular focus on the most prevalent orchards. Our method, which combines machine learning with Bayesian calibration, has proven effective in identifying more specific crops that are often present in particular regions and therefore underrepresented at the national level. By increasing the granularity of these subclasses in a LULC coarse dataset, this approach provides improved support for agricultural management, landscape planning, and related sectors, benefiting agricultural authorities, research institutions, and farmers. Additionally, the resulting mapped dataset is made publicly available, promoting broader applications and facilitating further research in agricultural monitoring and management.

1. Introduction

Accurate large-scale crop mapping is essential for global food security, reliable supply chains, and effective monitoring of environmental and economic changes (Tubiello et al., 2023; Teluguntla et al., 2015). Identifying crop types at regional and global scales with high spatial resolution reduces uncertainties in yield estimation and informs better planting decisions (Chen et al., 2018). Various Land Use and Land Cover (LULC) products currently provide detailed descriptions of land cover crop type, available at regional, national, continental, or global scales (Wang et al., 2023). Remote sensing plays a pivotal role in developing these products (Hütt et al., 2016; Kumar et al., 2022), leveraging satellites equipped with sensors of varying spatial, spectral, temporal, and radiometric resolutions (Zhang et al., 2020a) to offer a comprehensive and periodic view of the Earth's surface (Wang et al., 2023). The availability of vast amounts of geospatial data through cloud platforms has significantly facilitated the creation of extensive LULC products (Ahmed and N, 2023; Floreano and de Moraes, 2021; Tassi and Vizzari,

* Corresponding author.
E-mail addresses: f.lodato@unicampus.it (F. Lodato), jaynerya@msu.edu (R. Jayne), m.santonico@unicampus.it (M. Santonico), maurizio.pollino@enea.it (M. Pollino), flavio.bellino@roullier.com (F. Bellino), l.degara@unicampus.it (L. De Gara), basso@msu.edu (B. Basso).

https://doi.org/10.1016/j.srs.2025.100237
Received 7 October 2024; Received in revised form 6 March 2025; Accepted 17 May 2025
Available online 29 May 2025

2020). Developments in machine learning and deep learning techniques have enhanced the accuracy of these products, allowing for results that are tailored to specific applications and data types (Zhao et al., 2024; Shafizadeh Moghadam and Weng, 2021; Nigar et al., 2024; Pluto Kossakowska, 2021). Despite these advancements, many existing large scale LULC products fall short in providing the level of detail needed for identifying specific landscape elements (Xue et al., 2024), such as particular types of orchards. This limitation is often due to the resolution of the sensors used and the complexity of ground configurations, which can vary significantly due to different management practices, phenological phases influenced by varying climates, and annual changes in cloud cover (Wardlow et al., 2007; Wardlow and Egbert, 2008), moreover the crop spectral signature is often similar to spontaneous vegetation (Roy et al., 2018). For example, the Crop Data Layer (CDL) in the United States provides a high-resolution national scale crop mask at 30 m of resolution, reporting an accuracy exceeding 90 % for major crops, though its accuracy is limited for minor crops such as certain types of orchards (Boryan et al., 2011; Lark et al., 2021; Larsen et al., 2015). Current efforts are focused on enhancing the accuracy and reliability of this data (Lin et al., 2022; Maleki et al., 2024). In Europe, the EUCROPMAP 2018 (d'Andrimont et al., 2021) offers a 10-m resolution map of European crops, although it groups orchards with other permanent vegetation cover classes. Another significant European product is the CORINE Land Cover (CLC) program (Büttner et al., 2004), which maps land cover with an emphasis on agricultural areas, including olive groves and vineyards. However, the Corine Land Cover (CLC) minimum mapping unit of 25 ha is often inadequate to accurately capture important land uses at finer spatial resolutions, thereby limiting the effectiveness of analyses for specific agricultural practices and local management needs (Weissteiner et al., 2011), particularly in heterogeneous agricultural landscapes such as those found in Southern Europe (Ioannidou et al., 2022b), or in areas with significant intercropping (Mahlayeye et al., 2022). These limitations underscore the necessity for high-resolution spatial satellite surveys to accurately detect and analyze orchard presence. As previously discussed, sensor resolution remains a critical challenge. Although high-resolution imagery combined with Convolutional Neural Networks (CNNs) has shown promising results (Bouguettaya et al., 2022), scaling these techniques to large areas is often impractical due to the high cost of imagery and computational resources required (Jiang et al., 2020). Moreover, high-resolution satellites frequently lack sufficient spectral information, making it challenging to differentiate between similar crops based solely on texture (Fan et al., 2021). However, freely available satellite imagery, such as Sentinel-2, provides a 10-m multi-spectral images with an acquisition each 2–3 days at mid-latitudes with large-scale coverage. This includes spectral information in the shortwave infrared (SWIR) and red edge regions, which is critical for specific crop identification (Song et al., 2021; Zhang et al., 2020b; Lodato et al., 2024; Sasso et al., 2024). We can also leverage Sentinel-1's radar capabilities, which provide backscattering and polarization feature helpful for distinguishing different crops while avoiding cloud interference (Sahu et al., 2018). The data fusion of optical and radar data provides better results on crop type detection to a single source standalone (Sun et al., 2020; Ioannidou et al., 2022a; Orynbaikyzy et al., 2020; Inglada et al., 2016). The entire collections are now available on Google Earth Engine, a cloud-based platform that provides access to thousands of images at various levels of preprocessing (Gorelick et al., 2017). This platform enables efficient management of large datasets, allowing for rapid spatial and temporal analysis on a large scale. Such capabilities help to overcome traditional challenges in detecting specific crops within orchards at a national scale (Shelestov et al., 2017). By leveraging the spectral and temporal resolutions of these satellite collections, substantial aggregated information can be extracted (Carrasco et al., 2019). Applying machine learning and deep learning techniques to this extensive geospatial data allows for achieving accurate results (Yao et al., 2022). Numerous studies in the literature have explored large-scale classification of specific tree crops using remote sensing techniques. For instance, Zhang et al. (2023) mapped apple distributions across various regions of China by integrating UAV and Sentinel-2 imagery through a deep learning and transfer learning approach. This methodology has been extended by other researchers to classify mango, tea, and rubber plantations in India, leveraging the Random Forest algorithm and Sentinel-2A data (Pasha et al., 2023). Further advancements have been made in the mapping of tea plantations. Peng et al. (2024) proposed a method that incorporates satellite imagery along with socioeconomic and topographic variables, introducing a knowledge-based index sensitive to polyphenol content in tea leaves. Similarly, Toosi et al. (2022) developed an automated system for large-scale citrus detection in Iran, utilizing NDVI time series in combination with satellite imagery. In the context of olive tree segmentation, Abozeid et al. (2022) introduced a specialized architecture tailored for high-resolution image analysis. For vineyard mapping, Özlem et al. (2024) applied a 3D convolutional neural network to high-resolution imagery, successfully mapping vineyards across a vast area of Turkey. Beyond specific crops, Nabil et al., 2022. focused on the classification of multiple woody crops in the Nile Delta using a combination of optical and radar data, achieving high accuracy with the Random Forest algorithm. In southern France, Abubakar et al. (2023) delineated olive groves and vineyards by analyzing Sentinel-2 derived products and phenological metrics, also employing the Random Forest algorithm with good results. Currently, there is a lack of national-scale classification of the primary cultivated tree species in Italy. Given the significant economic impact of the fruit orchard sector, both productive and landscape-oriented (Costantini and Barbetti, 2008; Corsi et al., 2019; Stillitano et al., 2016), it is essential to develop a tool to monitor and analyze the area covered by orchards. The aim of this study is to develop an advanced pipeline for the precise mapping of Italy's primary cultivated orchards at a national scale, with a spatial resolution of 10 m. This objective will be accomplished by reclassifying the CORINE Land Cover agricultural classes (specifically the 2.x classes) through a integration of satellite imagery, machine learning algorithms, and statistical modeling supported by data from the national statistical system. A comparison between the efficacy of machine learning models alone versus the combined approach incorporating statistical methods is tested. The results demonstrate a marked improvement in accuracy when statistical modeling is employed alongside machine learning. The final, high-resolution dataset will be made available to stakeholders, providing a critical resource for the ongoing monitoring and management of Italy's orchard landscapes.

2. Study area and data

2.1. Area of interest (AOI)

This study was conducted in Italy, a Mediterranean country known for its elongated shape and a wide range of environments, microclimates, agricultural systems, and local traditions, all of which contribute to a high degree of diversity (Dal Ferro and Borin, 2017). For the purposes of this research, all areas classified under class 2 (Agricultural areas) from the CORINE Land Cover (CLC) 2018 dataset were extracted, with the exclusion of subclasses 213 (rice fields), 231 (pastures), and 244 (agroforestry areas). The CORINE Land Cover layer was acquired from Earth Engine with a resolution of 100 m and a Minimum Mapping Unit (MMU) of 25 ha. This process resulted in an Area of Interest (AOI) of approximately of 130,000 km^2, entirely within Italian territory (Fig. 1).

2.2. Statistical data

Prior the study, an investigation was conducted to identify the most relevant orchards in terms of production area in Italy. This involved consulting the national statistical system to extract data on production areas for each crop in 2022 (Istat, 2022). This allowed us to identify the

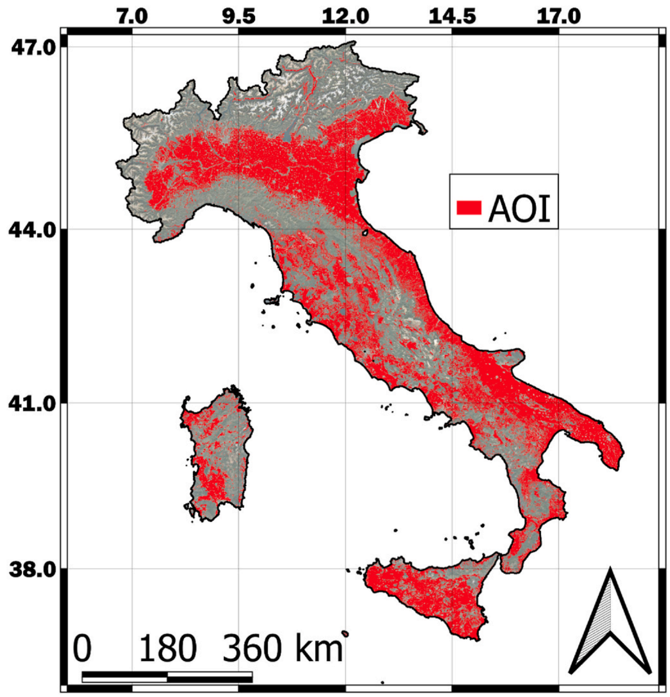

Fig. 1. Area of Interest (AOI), highlighting the areas extracted from the CLC.

most representative fruit tree species across the Italian territory, including:

1. **Olive (Olea europaea) (OLI):** The olive tree, cultivated both for oil production and as a table fruit, is the most widespread tree crop in Italy, covering an estimated 1,120,000 ha nationwide. As a distinctly Mediterranean species, it is predominantly found in the southern regions of Italy, where it has traditionally been grown in hilly and marginal areas due to its adaptability (Bartolini and Petruccelli, 2002). In recent years, however, its cultivation has expanded into plain areas, often with intensive row planting systems (Stillitano et al., 2017). It is important to note that olive groves, which have been cultivated for centuries, often consist of large, irregularly planted trees. These groves may sometimes appear only as perimeter plantings or within polycultural systems, complicating their identification as discrete "olive groves." The species is evergreen, displaying a unique temporal growth pattern that distinguishes it from other crops.
2. **Vineyard (Vitis vinifera) (VIN):** Vineyards play a crucial role in the agro economic development and landscape of Italy (Torquati et al., 2015). Grapes are cultivated across the entire country, from north to south and from east to west, encompassing a wide range of varieties and cultivars. The management of vineyards varies significantly (Cogato et al., 2020), with traditional row plantings prevalent throughout Italy and canopy arrangements (such as "pergola" or "tendone") more common in southern regions. In some cases, vineyards in the south are covered with plastic fabrics to protect the grapes. Vineyards, whether for wine production or table grapes, represent the second most widespread tree crop in Italy, covering an estimated area of 736,000 ha.
3. **Stone Fruits (S.F.):** This category includes all stone fruits such as peaches (Prunus persica), apricots (Prunus armeniaca), plums (Prunus domestica), cherries (Prunus avium), and almonds (Prunus dulcis). These crops follow a similar phenological phase, with a period of vegetative rest, spring flowering, and a summer vegetative phase. Collectively, they represent the third most extensive tree crop in Italy (estimates 173,000 h), with some polarizations and districts of excellence.
4. **Citrus (CIT):** The citrus class encompasses all citrus fruits, including oranges (Citrus sinensis), lemons (Citrus limon), mandarins (Citrus reticulata), citrons (Citrus medica), bergamots (Citrus bergamia), and a small percentage of less common citrus varieties. The cultivation of these CIT fruits is primarily concentrated in southern Italy. All these species are evergreen, which results in a specific spectral and temporal pattern. CIT fruits collectively rank as the forth most widespread tree crop in Italy, with an estimated surface area of 120,000 ha.
5. **Apples (Malus domestica) (APP):** Apple cultivation in Italy is highly polarized, primarily occurring in compact row systems often covered with hail protection nets. Approximately 95 % of apples in Italy are produced in the valleys of the Trentino-South Tyrol region, where the apple finds its climatic optimum, leading to the development of a true agro-industrial system. However, there are also specialty apples from typical regions, such as the Annurca apple, which is cultivated in the Campania region using traditional planting systems rather than narrow, high rows. This results in a different temporal pattern due to varying climatic conditions. The apple estimated surface in Italy is 56,000 ha.
6. **Pears (Pyrus) (PEA):** Like apples, Pear cultivation in Italy is highly polarized in a very restricted area in the Emilia Romagna region where specific areas of vocation exist. Pears are grown in tall rows suitable for collection via harvesting cart, with a smaller surface area compared to other crops and a decreasing trend, with an estimate surface of 26,000 ha.
7. **Actinidia (Actinidia deliciosa) (ACT):** Actinidia (Kiwifruit) cultivation is relatively recent in Italy and, like apples and pears, is highly polarized in certain districts. In particular, a significant percentage of kiwi production in Italy comes from the provinces of Latina and Cuneo. The cultivation system is a standard canopy often covered with protective plastic fabric. The estimates surfaces covered by actinidia is 25,000 ha.

Once the classification classes were established, the original statistical dataset was divided by province. For each province, the percentage of coverage for each orchard class relative to the total agricultural area was calculated.

2.3. Ground truth

For the ground truth polygons, we relied on information from Timac Agro Italia, which operates nationwide. Starting with the company polygons and using the statistical dataset, we aimed to select a significant number of polygons for each Italian province. For some provinces, no polygons were available, which was due to a lack of fruit cultivation in the area. A total of 3015 OLI polygons, 3232 VIN polygons, 633 CIT polygons, 595 S.F. polygons, 390 APP polygons, 232 ACT polygons, and 247 PEA polygons were collected (Supplementary Fig. 1).

2.4. Satellite data

For the satellite data, a technique similar to that used in (Lodato et al., 2024) was employed, which has proven effective in recognizing specific perennial crop patterns by leveraging a large volume of information from multiple satellite sources and aggregating the data temporally. For the optical data, we utilized the S2_SR_Harmonized collection, which provides Sentinel-2 surface reflectance data available on Google Earth Engine (GEE) (ESA, 2023a). This collection was clipped to the area of interest (AOI) and a cloud mask was applied to remove cloudy pixels. The collection includes various bands, such as RGB bands (B2, B3, B4), Red-Edge/NIR bands (B5, B6, B7, B8, B8A), and SWIR bands (B11, B12). Bands 1 (Aerosol) and 9 (water vapor) were excluded due to their larger pixel sizes, which are less suitable for crop detection. The dataset was filtered to include images from January 2021 to December 2023 and divided into 12 collections, one for each month.

Thus, each monthly median value for the bands is calculated based on the reflectance data from all three years (2021, 2022, and 2023). For example, the median value for Band 2 in January is derived from the median of all Band 2 reflectance values collected over January 2021, 2022, 2023. This approach helps mitigate random factors due to local or widespread conditions, such as drought or excessive pruning, ensuring more robust data for modeling. This process yielded to 120 bands, forming optical dataset. For Sentinel-1 radar data, we utilized the GEE Copernicus S1_GRD dataset in Interferometric Wide-swath (IW) mode (ESA, 2023b). We selected only images that partially or wholly intersected the AOI for the year 2023, focusing specifically on ascending orbit images and the VV and VH backscattering bands. To mitigate speckle noise while retaining essential image features, a 3 × 3 pixel Lee Filter was applied to the entire collection. To address variations in backscatter caused by fluctuations in incidence angle, we implemented Square Cosine Correction based on Lambert's law. This correction used the mean incidence angle of each image within the AOI as a standardizing factor. Subsequent processing steps included conversion to linear units, monthly averaging, and conversion back to decibels. This process yielded 24 images, forming the radar dataset. The bands from the optical and radar collections were then stacked, resulting in a unified data cube of 144 bands for the entire AOI (Fig. 2). This data is accessed via server requests rather than being downloaded directly.

2.5. Sampling methods and points

After establishing the reference dataset for the entire AOI, sampling points were extracted (Fig. 3). A negative buffer of 20 m was applied to each polygon to eliminate edge effects. Once buffering was complete, a random number of points was generated within each polygon. This number was determined by multiplying the specific rounded number of hectares of each polygon by 5, with a minimum spacing of 30 m between points. This method ensured approximately one sampling point for every 2000 square meters of the field.

The sampling scale size was subsequently determined (Fig. 4). One-third of the pixels were randomly selected to capture the spectral-temporal signature at 10 m, another third at 20 m, and the final third at 30 m. Referring to the Earth Engine documentation, the "scale" parameter was used to set the sampling size. Earth Engine employs a pyramidal system for data assembly. At 10 m, the pixel retrieves the array of data from the pixel it falls within, being the resolution of the reference dataset at 10 m. Using scales of 20 and 30 m, Earth Engine performs an interpolation based on the nearest neighbour using Euclidean distance, aggregating 4 and 9 pixels respectively for sampling at 20 and 30 m.This provides a value calculated with the nearest neighbour method. Consequently, at 20 and 30 m, the sampling point does not simply retrieve the array of values from the pixel it falls within, but rather from aggregated pixels within the field.

Sampling at different scales allows for more generalized spectral-temporal signatures that account for significant intra-field variability. For classification, an "Other" (OTH) class was added to differentiate areas that are not orchards from the selected categories. This class serves as a background category in the machine learning model, helping the algorithm identify and filter out non-relevant areas. To define this class,

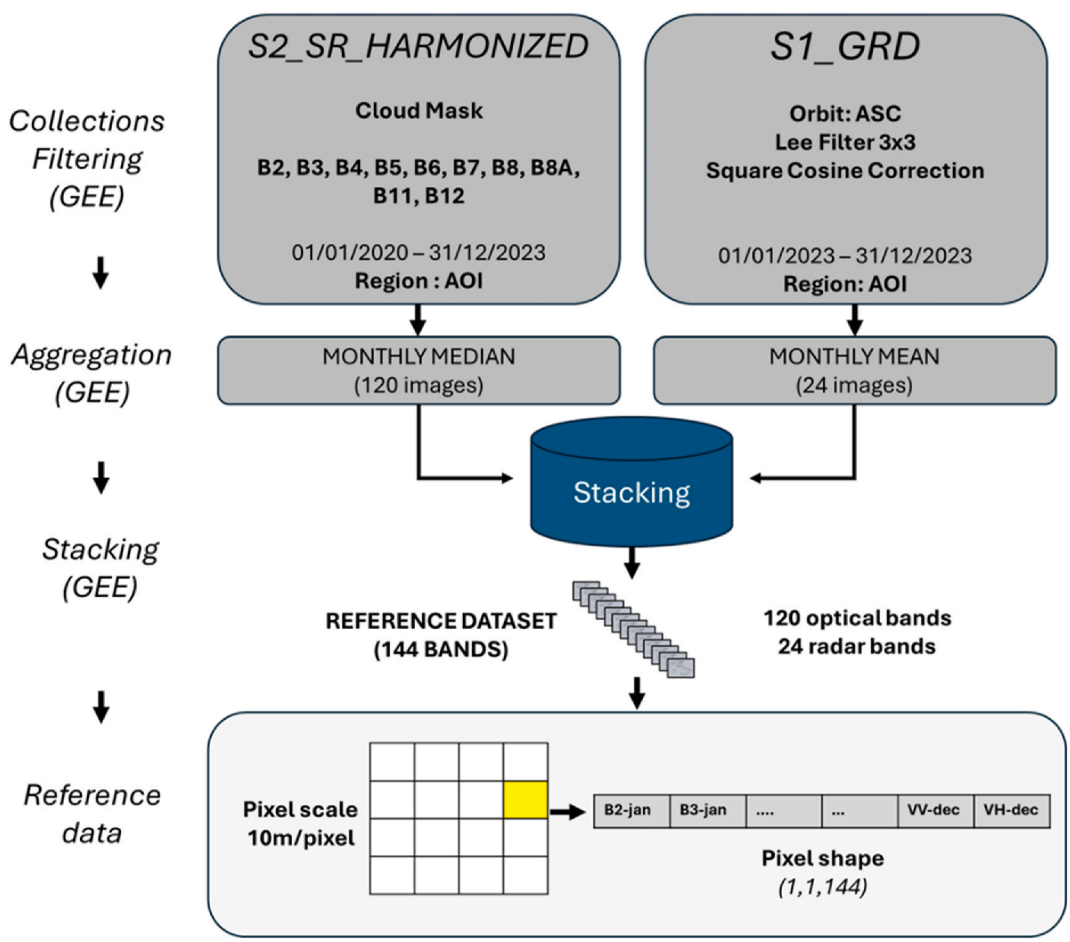

Fig. 2. The two collections were processed with specific filtering in the Google Earth Engine platform. Preprocessing was applied, and the data was reduced to a monthly resolution before performing a single stacking. By the end of the process, the datacube for the area of interest (AOI) comprises 144 bands, including 120 optical and 24 radar bands.

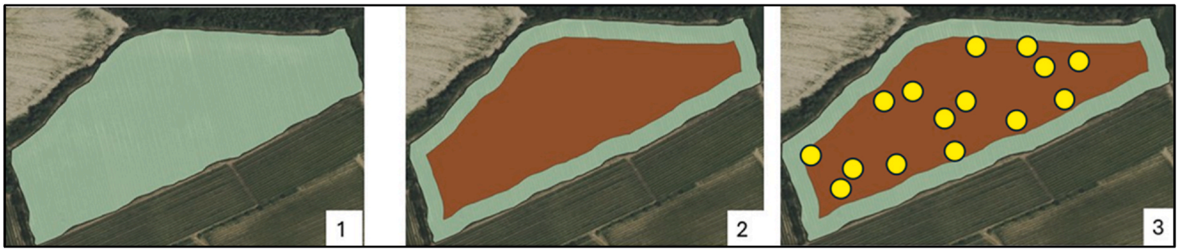

Fig. 3. In step 1, an original VIN polygon is shown. In step 2, the polygon is subjected to a 20- meter negative buffer to address edge effects. In step 3, a number of sampling points is generated, calculated as the number of hectares (in this case, 3) multiplied by 5, with a minimum spacing of 30 m. This results in a total of 15 sampling points for this example.

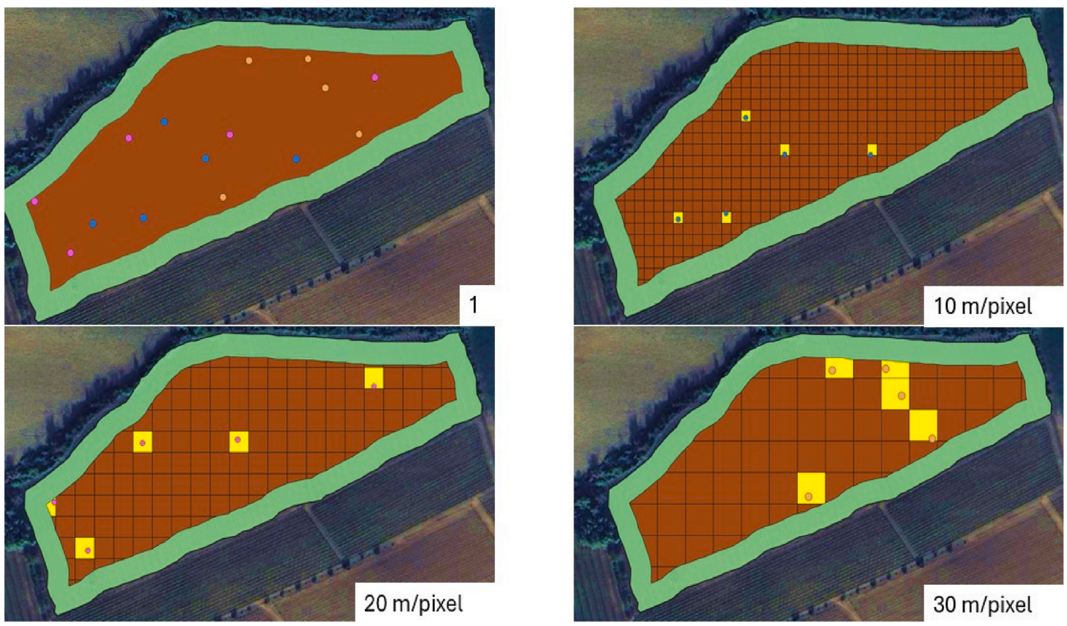

Fig. 4. In the first image, the sampling pixels are randomly divided into three subsets. The second image illustrates how sampling is conducted on a 10-m grid using a scale factor of 10, which corresponds to the base resolution of the dataset. This is followed by sampling at 20 m using a scale factor of 20, and at 30 m using a scale factor of 30.

spectral signatures were collected from various sources, including other types of crops like arable land and chestnut trees, as well as urban and aquatic environments using data from the CORINE Land Cover. Additionally, polygons from forested and riverine areas were included. This process resulted in a total of 60,326 background training points. The training dataset thus consists of a total of 169,836 (Table 1) sampling points.

3. Classification methods

For the classification of the entire Area of Interest (AOI), a two-step approach was implemented (Fig. 5). In the first step, an XGB machine learning model was trained using training points. This model classified the entire AOI by generating a probability score for each pixel, rather than making a definitive categorical prediction. The output is comprised of eight layers, each representing the probability of individual pixel belonging to specific classes. In the second step, a Bayesian approach was employed to calibrate the predicted probabilities. This process outputted probabilities from the XGB model as independent variables and national statistical data as Bayesian priors. The Bayesian calibration step biased the probabilities of each classification according to the proportions of each crop type within each Italian province. Subsequently, an argmax operation was performed to assign each pixel to the class with the highest probability, which is the final classification. For provinces without polygons or with a negligible proportion of orchards (less than 3 % of the total land cover), the argmax result from the XGB model was applied directly. The rationale for using a two-step classification approach lies in the inherent characteristics of discriminative machine learning algorithms, which are fundamentally data-driven and focus solely on mapping input features to classifications. Models such as XGB are particularly adept at identifying patterns within data and achieving high accuracy classification (Chen and Guestrin, 2016). However, these models are limited in their ability to model the joint probability distribution of input features and classifications (Ng and Jordan, 2001). As a result, discriminative models may not capture the

Table 1
Number of sampling points for each class.

Class	n
OLI	35,906
VIN	32,345
CIT	14,344
APP	12,302
S.F.	12,046
PEA	9638
ACT	5231
OTH	60,326
Total training points	**169,836**

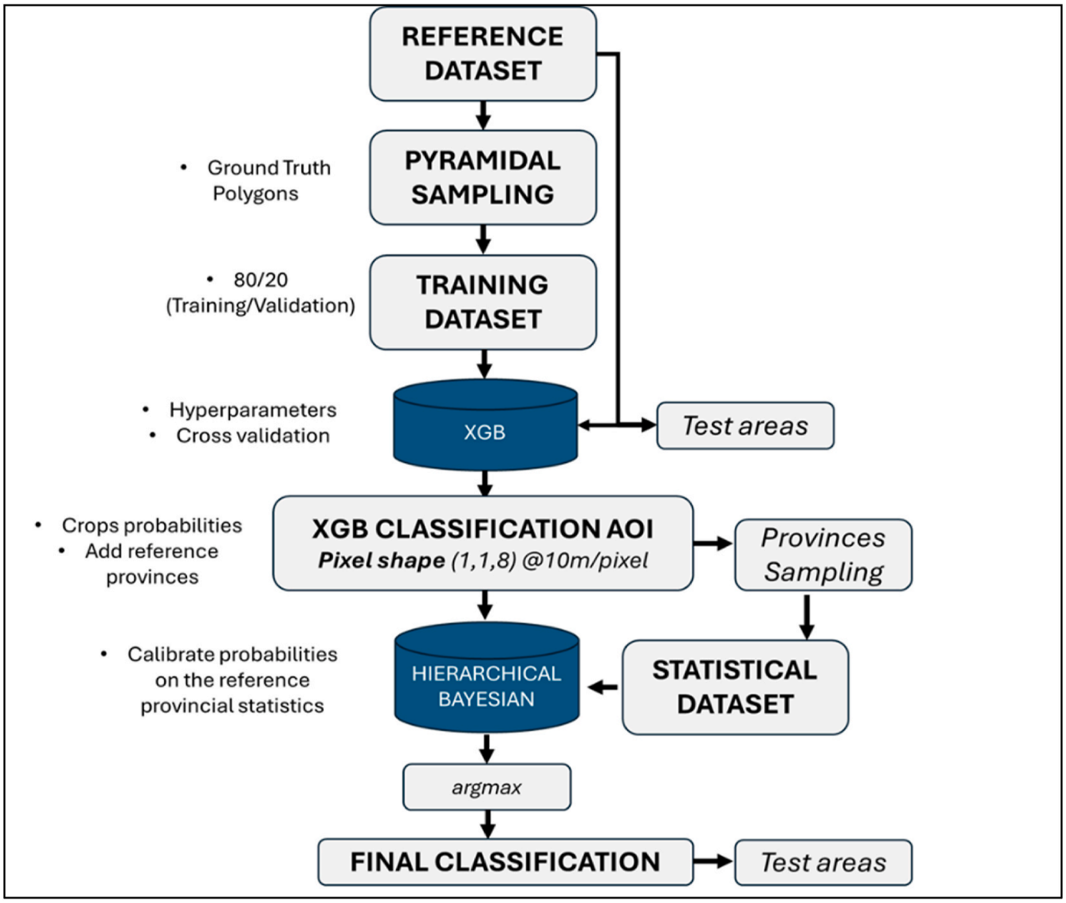

Fig. 5. Classification pipeline overview. Sampling points with labels are extracted from the polygons in the reference dataset. These are used to train an XGB model, which, after hyperparameter optimization, classifies the entire AOI at a 10m/pixel resolution, generating eight layers representing the probability of each pixel belonging to a specific class. In the second step, a hierarchical Bayesian model is applied to recalibrate these probabilities. This model uses national crop coverage data to adjust the proportions and ensures the classification aligns with provincial distributions. The final classification is achieved by performing an argmax operation on the recalibrated probabilities.

nuances of low-probability classifications under certain conditions as effectively as generative models. To enhance the calibration of these probabilities, techniques such as Platt scaling and isotonic regression are commonly used. These methods have proven to be effective, especially in bagging and ensemble algorithms (Sweidan and Johansson, 2021). However, calibration techniques primarily focus on adjusting the model's output based on test data. A significant limitation is that the available test data may be limited, and the calibration process relies on the errors observed within this data. Incorporating a Bayesian classifier, which integrates prior knowledge, can significantly improve the final prediction. This integration allows for the consideration of additional factors and reduces uncertainty in probability estimates, resulting in more robust and accurate models. In Italy, crop distributions are heavily influenced by agroecological and cultural farming factors, leading to varying prevalences of specific crops across different regions. Due to the challenges of integrating this information directly into the XGB algorithm, we propose incorporating prior information within a hierarchical Bayesian framework. This approach introduces probabilistic bias into the classifications produced by the XGB model based on provincial crop/tree proportions, providing an additional model layer that aligns classification probabilities more closely with their true regional distributions. To evaluate the performance of the classifiers, we use the following metrics:

- **Recall** (or sensitivity) quantifies the model's ability to correctly identify positive instances of a class:

$$Recall = \frac{TP}{TP + FN}$$

A high recall indicates that the model successfully identifies most true positive instances without missing any.

- **Precision** measures the accuracy of positive predictions:

$$Precision = \frac{TP}{TP + FP}$$

High precision indicates that the model minimizes false positives, accurately classifying the positive instances.

- **Overall Accuracy** represents the proportion of correctly classified instances:

$$OA = \frac{TP + FN}{TP + TN + FP + FN}$$

This metric reflects the overall correctness of the classification, but it may be misleading in the presence of imbalanced data.

- **F1 Score** provides a balance between precision and recall:

$$F1 = 2 * \frac{Precision * Recall}{Precision + Recall}$$

This metric offers a evaluation by considering both precision and recall, useful for assessing the performance of a classifier on a specific class.

3.1. Probabilistic XGB (XGB)

For the first step of classification, we use the XGB classifier (Chen and Guestrin, 2016). This algorithm falls under the supervised machine learning category and can handle both classification and regression tasks. XGB is an ensemble non parametric algorithm that relies on a robust decision made by multiple "weak" classifiers, which in this case are decision tree-based algorithms. Unlike other ensemble algorithms, XGB utilizes gradient boosting (Friedman, 2001) to iteratively train a series of decision trees. Each subsequent tree aims to correct the residual errors of the previous models. This iterative approach makes XGB extremely effective in reducing loss across iterations. In addition, XGB offers several loss functions tailored to different types of objectives. It features a comprehensive set of adjustable hyperparameters for mitigating overfitting through regularization. Moreover, its capability for parallelization enhances its speed and usability. These features have made it renowned across various ML contexts, delivering high performance in benchmarks and finding extensive use in many remote sensing applications such as urban impervious surface extraction (Shao et al., 2024), land use and change (Bhagwat and Shankar, 2019; Arfah et al., 2021), tree species classification (Łoś et al., 2021; Zhou et al., 2022), crop type mapping (Prins and Van Niekerk, 2021) even in heterogeneous agricultural environments (Saini and Ghosh, 2021). In our case, as default, we opted to use the model with the "softprob" loss function, which returns the predicted probability of each data point belonging to each class. To evaluate accuracy during validation, we employed the "mlogloss" metric (Multiclass Log Loss). This metric quantifies the accuracy of multiclass classification models by assessing the logarithmic discrepancy between predicted probabilities and actual class labels. Training and Validation set was split in a stratify 80/20 set and to correct class imbalance, each sample in the training dataset was weighted using a "balanced" function. This function automatically adjusts the weights inversely proportional to class frequencies. This approach mitigates the imbalance among classes and ensures a more balanced output. Subsequently, hyperparameter optimization of the model was conducted, with particular attention paid to constraining parameters during the grid search to prevent overfitting:

- **max_depth**: maximum depth of a single tree, this parameter goes from 1 to infinity. A lower depth can lead to underfitting, while higher values lead to overfitting model. This parameter is related to the number of predictors which in this case is high. To contain overfitting, the parameter search was maintained low: [5, 10, 20, 30].
- **min_child_weight**: specifies the minimum amount of observations required in each leaf node of the tree, this parameter goes from 1 to infinity. Higher values of this parameter can help to regularize the model preventing overfitting [10, 20, 50, 100].
- **subsample**: This parameter sets the fraction of observation in each tree, this value ranges from 0 to 1. Setting this parameter high leads to overfitting, so the data range was set to [0.4, 0.5, 0.6].
- **colsample_bytree**: is the ratio of the predictor used when constructing each tree, with a range from 0 to 1. Setting this parameter high leads to overfitting, parameter searched [0.4, 0.5, 0.6].
- **eta (learning_rate, shrinkage)**: controls the step size at which the optimizer makes updates to the weights. This value ranges from 0 to 1, lower values help the model to converge, but significantly slow down the training time. In grid search we use [0.001, 0.01, 0.02, 0.05, 0.1, 0.2, 0.3].
- **num_estimators**: this parameter sets the number of trees in the model, can range from 1 to infinity. Higher values of trees increase the complexity of the model leading to better prediction but can lead to overfitting and harder computation. Range used [100, 200, 300, 400].

Hyperparameter tuning was performed using 10-fold cross-validation. After finding the best hyperparameters, the entire Area of Interest (AOI) at 10m/pixel was classified. The hyperparameters for the XGB model, optimized through cross-validation, are summarized in Table 2.

3.2. Hierarchical Bayesian model (HB)

In this section, we explain our approach to improving the probabilistic classifications generated by the XGB algorithm using a hierarchical Bayesian model. XGB produces predictions by summing the contributions of decision trees, each weighted by a learning rate, across multiple iterations. These predictions result in a vector of class scores for each crop type, which are then converted into probabilities using the SoftMax function. To enhance these classifications, our hierarchical Bayesian model incorporates provincial crop proportions as prior knowledge, allowing for more accurate and region-specific predictions. Our hierarchical Bayesian model utilizes XGB-generated features to estimate both global covariates and region-specific crop type intercepts. This model is structured as a multinomial logistic regression, where the intercepts are informed by the regional proportions of crop types. To formalize the priors, we use a Dirichlet distribution for the regional crop proportions, reflecting high confidence in the known distributions, while the covariates' priors are normally distributed with a moderate degree of informativeness. Variational inference is applied to approximate the posterior distributions of the model parameters, providing a more tractable and computationally feasible solution for probabilistic crop type classification, as often opposed to Markov Chain Monte Carlo (MCMC) methods (Blei et al., 2017). The XGB algorithm generates classifications of the form:

$$\widehat{w_i} = \sum_{t=1}^{T} \alpha f_t(x_i) \tag{1}$$

where $\widehat{w_i}$ is the predicted class category, α is the learning rate that scales the contribution of each decision tree, and $f_t(x_i)$ is a function at the t-th iteration and x_i is a vector of the input features at the i-th instance. Each $\hat{w_i}$ produces a vector of scores per class category as:

$$\widehat{w_i} = \left[w_{i1}, w_{i2,} \dots w_{ik}\right] \tag{2}$$

where k is the number of class categories. Finally, the vector of scores is passed through a softmax function that converts the scores to probabilities, giving:

$$P(w_i = k|x_i) \tag{3}$$

where the classification is decided based on which class category has the highest probability. We designed a hierarchical Bayesian model to make crop type classifications by taking the outputs from the XGB that considers the crop-type labels given the inputs. we use 97 different provinces, as some of the province was missing polygon ground truth data or with very low coverage of orchard, thus we take a matrix of class category proportions for each crop type with dimensions 97×8, where $k = 8$, which defines the context of the model about how we can include prior information to bias our classifications. The general form of the hierarchical Bayesian model uses a feature matrix of the XGB outputs to estimate global-level covariates and region-varying crop-type intercepts

Table 2
Hyperparameters used for the XGB model.

Parameter	Value
Max Depth	20
Min Child Weight	50
Subsample	0.5
Colsample Bytree	0.6
Learning Rate (Eta)	0.005
Number of Estimators	200

estimated from the regional crop proportions. The model form is a multinomial logistic regression with region-varying intercepts and global, crop-type varying covariates:

$$\hat{y}_{ir} = \alpha_{r[i]k} + X\beta_{ik} = \alpha_{r[i]k} + x_1\beta_{i1} + x_2\beta_{i2} + \ldots + x_k\beta_{ik} \tag{4}$$

where $\hat{y}_{ir}$ is the final prediction of pixel classification for pixel i in region r, and $\alpha_{r[i]k}$ is a region-varying intercept that biases the classification of the i^{th} pixel by setting its initial class logit of the crop-type k to the proportion of its region r. The subscript $r[i]k$ is meant to denote the i^{th} observation in region r, where k refers to the logit for crop k. The matrix $X \in R^{Nxk}$ contains the features from the outputs of the XGB algorithm. To incorporate our prior information about regional crop proportions and the features generated from the XGB model, we define the prior distributions as follows:

$$a_r \sim Dirichlet(p_{rk}, 10) \tag{5}$$

$$\beta_{f,k} \sim Normal(0, 0.1) \tag{6}$$

We set informative priors on α, which uses a Dirichlet distribution where the proportion of each crop k in region r is set to true proportions of the region and with a concentration parameter equal to 10 to reflect high confidence in this prior. For the global-level covariate weights, $\beta_{f,k}$ where f represents the feature and k represents the crop type, we set the prior mean equal to zero with a standard deviation of 0.1 to be a moderately informative prior. Our justification for this is because the XGB classifications are already generating high accuracy.

Finally, the likelihood function models the probability of observing a particular crop type given the features and regionally varying crop type proportions. Per observation i, we have k logits,

$$P(y|X,\alpha,\beta) = \prod_{i}^{N} Multinomial(y_i|softmax(logits_i)) \tag{7}$$

where the logits for observation i in region r are defined as,

$$logits_i = \alpha_{r[i]k} + X\beta_{ik} \tag{8}$$

We use variational inference to approximate the posterior distributions of our parameters, $p(\alpha,\beta|y,X)$ by maximizing the Evidence Lower Bound (ELBO) criterion to make probabilistic inferences on the classifications. This approach provides a more flexible method for estimating posterior distributions by approximating them with a simpler, tractable distribution (Blei et al., 2017). Hence, the final classification is based on the logit corresponding to crop type k for the given i-th observation.

3.3. Test areas

Upon completion of the model application, the entire Area of Interest (AOI) was classified using the XGB + HB model. To validate the approach, field surveys were conducted to obtain ground samples from various locations. Each site was examined to identify the range of crops present, with attention to areas containing multiple crop types. This was done to assess the model's capability to discriminate among different crops and to determine if the two-stage classification approach was consistent, or if the statistical method disproportionately favored the dominant crop in the region. Additionally, a false positive test was performed in a non-agricultural area within the AOI, including both fallow and forested regions, to evaluate the occurrence of false positives in the background class. The first test (Fig. 6A) was conducted in the Trani-Barletta-Andria province (Puglia Region, Southern Italy). The proportions in the national-level statistical dataset reveal an abundant presence of olive groves, covering 39 % of the agricultural area in the region. This is followed by 34 % of areas cultivated with other crops (OTH), 22.5 % of VIN, 4.5 % of stone fruit. The test area presents homogeneous proportions of OLI, VIN, and stone fruit, with a total of 0.50 km^2, of which 19 % are represented by interstitial or uncultivated areas. The aim of this test was to evaluate the ability of the two methods to identify a crop underrepresented in the provincial proportions, as in the case of stone fruit, while also assessing the effectiveness in discriminating the more dominant crops. For the second test area (Fig. 6B), a region with two equally dominant crops in the territory was chosen, in the province of Trento (North-Eastern Italy), which has 42 % apples and 42 % VIN, with a minimal area dedicated to other crops (about 3 % distributed among the other classes and 12 % of OTH). The purpose of this test is to evaluate the effectiveness of discrimination based on two equally present crops in the territory, but not in the training data. The ground-classified area is 0.5 km^2 and consists of 45 % apples, 25 % VIN,

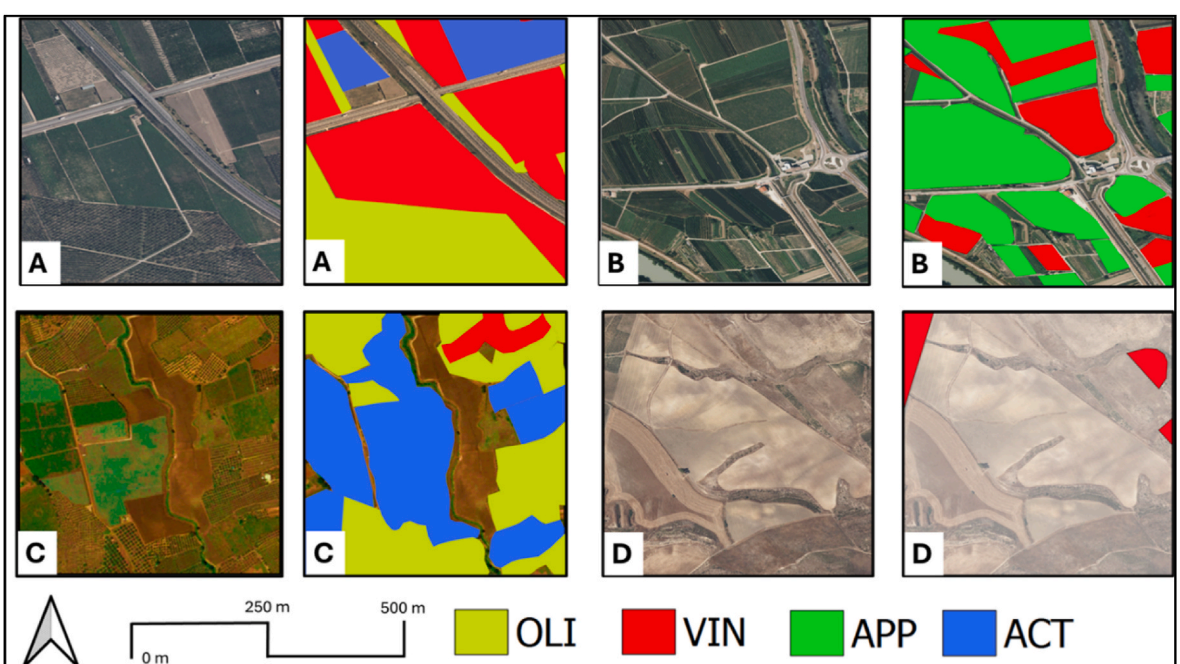

Fig. 6. Test areas and corresponding ground truth masks. (A) Test Area 1, (B) Test Area 2, (C) Test Area 3, and (D) Test Area 4.

and 30 % OTH. In the third test (Fig. 6C), the models' ability to detect a crop that is strongly underrepresented in the training dataset was evaluated, in this case, ACT, which finds its maximum concentration in the province of Latina (Lazio Region, Central Italy) with 10.7 % of agricultural coverage, compared to 19 % of olive groves, 7 % of VIN, about 1 % distributed among other orchards, and 62 % of OTH. The aim of this test is to evaluate whether the model can effectively use the probabilistic approach to improve the prediction of a class strongly underrepresented in the training data. The area contains large quantities of ACT, in various growth stages (young and mature plants), and some covered with plastic roofing. The test area consists of 35 % ACT, 37 % olive groves, 24 % OTH, and 4 % VIN, totaling approximately 0.5 km^2. Finally, a false positive test was conducted (Fig. 6D). Starting from a province with an abundant presence of vineyards, an area covered primarily by arable land and wooded areas was classified to evaluate the HB classifier's tendency to force classification toward a crop rather than the background class. The province of Trapani (Sicily Region) was chosen for this area, which stands out for its quantity of VIN (52 % of the territory), 27 % OLI, and the remainder in the OTH category. The area presents as a vast field of arable land with VIN on the sides. with some interstitial areas featuring spontaneous vegetation.

4. Results

4.1. Accuracy metrics for validation dataset

The XGB alone achieved an overall accuracy (OA) and a weighted F1 score of 0.90 in validation (Table 3). Overall, the model exhibits accuracy and a weighted F1 score of 0.9, with a balance between precision and recall. The classifier achieved higher recall than precision for all crops except for the OTH class. The best results were obtained for ACT, apples, and pears. CIT, OLI, and VIN followed, maintaining an F1 score above 0.9. The implementation of the statistical method XGB + HB has produced excellent results in terms of accuracy metrics, almost always reaching 0.99. The confusion matrix (Supplementary Fig. 2) reveals that for XGB alone, except for the OTH class, misclassification among the various crop types is relatively low. However, there is a significant number of false positives where samples originally classified as OTH are incorrectly categorized as S.F., OLI, and VIN.

4.2. Test area 1

In Test Area 1, the model reported an overall accuracy of 0.76 for the XGB model and 0.83 for the XGB + HB model. Table 4 shows that for the OTH class, the XGB + HB model achieved a precision of 0.95 and a recall of 0.57, with an F1 score of 0.71. In contrast, the XGB model exhibited lower accuracy, with an F1 score of 0.51, a recall of 0.46, and a precision of 0.57. Among the orchard classes, the OLI class stands out with an F1 score of 0.91 for the XGB + HB model and 0.84 for the XGB model, for both models, recall was higher than precision. The VIN class follows in accuracy, with an F1 score of 0.85 for the XGB model and 0.82 for the XGB + HB model, showing similar values, and both models show a comparable ratio between precision and recall. For the S.F. class, the F1 score does not differ between the two models. However, while the XGB model alone shows a narrow gap between precision and recall, the gap is wider for the XGB + HB model. The analysis of the confusion matrices (Supplementary Fig. 3) show that both models achieve strong performance. However, a common issue is the frequent misclassification of the OTH class as an orchard by both models. Among the dominant crops, the XGB + HB model shows a slight edge in overall accuracy. Some misclassifications were observed, particularly where OTH pixels were incorrectly identified as VIN. Regarding the spatial distribution of misclassifications (Supplementary Fig. 4), both models frequently show errors along the borders separating fields or between crops and the OTH class. Notably, the XGB model exhibits a more concentrated spatial error pattern, where entire parcels or sections are misclassified as OTH rather than as crops (see Table 5).

Table 3
Models metrics for each crop on validation dataset.

	XGB + HB			XGB		
	Precision	Recall	F1-Score	Precision	Recall	F1-Score
ACT	0.98	0.97	0.97	0.96	0.99	0.97
APP	0.98	0.99	0.99	0.92	0.99	0.95
CIT	1.00	0.99	1.00	0.87	0.98	0.92
OLI	0.99	0.99	0.99	0.89	0.93	0.91
OTH	0.99	0.99	0.99	0.97	0.84	0.90
PEA	0.99	0.99	0.99	0.91	0.99	0.95
S.F.	1.00	0.98	0.99	0.69	0.94	0.80
VIN	0.99	0.99	0.99	0.88	0.92	0.90
Accuracy	**0.99**	**0.99**	**0.99**	**0.90**	**0.90**	**0.90**
Macro Avg	0.99	0.99	0.99	0.89	0.95	0.91
Weighted Avg	0.99	0.99	0.99	0.91	0.90	0.90

Table 4
Metrics for XGB + HB and XGB models in Test Area 1.

Model	Class	Precision	Recall	F1 Score
XGB + HB	OTH	0.95	0.58	0.71
XGB + HB	S.F.	0.61	0.89	0.72
XGB + HB	OLI	0.88	0.95	0.91
XGB + HB	VIN	0.85	0.85	0.85
XGB	OTH	0.57	0.46	0.51
XGB	S.F.	0.69	0.77	0.73
XGB	OLI	0.78	0.92	0.84
XGB	VIN	0.85	0.78	0.82

Table 5
Metrics for XGB + HB and XGB models in Test Area 2.

Model	Class	Precision	Recall	F1 Score
XGB + HB	OTH	0.91	0.47	0.62
XGB + HB	APP	0.83	0.93	0.88
XGB + HB	VIN	0.53	0.90	0.67
XGB	OTH	0.92	0.65	0.76
XGB	APP	0.90	0.52	0.66
XGB	VIN	0.37	0.93	0.53

4.3. Test area 2

In Test Area 2, the XGB model alone achieved an overall accuracy of 0.65, compared to 0.75 for the XGB + HB model. In terms of F1 score, the XGB model performed better for the OTH class. However, it showed poorer results for the VIN and APP crops, with lower F1 scores and low precision for the VIN displaying a large gap between precision and recall (Table 5). On the other hand, the XGB + HB model performed better with higher F1 scores for the APP class and higher precision for the VIN although precision remained generally low for this category. The confusion matrix (Supplementary Fig. 5) analysis reveals that the XGB model struggles to distinguish between APP and VIN with a high rate of underclassification where apples are incorrectly classified as VIN. Meanwhile, the XGB + HB model better discriminates these crops but has a substantial amount of false positives for VIN where other classes are overclassified as VIN. Notably, a small portion of VIN is misclassified by XGB as ACT. The spatial error analysis (Supplementary Fig. 6) indicates that a significant portion of the misclassifications by the XGB + HB model arises from border effects. These errors are concentrated along the boundaries of fields, creating a linear distribution pattern. In contrast, the XGB model frequently misclassifies entire plots, often substituting one crop type for another or misassigning them to the OTH category.

4.4. Test area 3

In Test Area 3, the performance evaluation revealed significant differences in overall accuracy between the two methodologies. The XGB + HB model demonstrated superior efficacy, attaining an overall accuracy of 0.79 compared to 0.44 achieved by the standalone XGB model. The XGB + HB model excelled in accurately classifying the class ACT and OLI (Table 6). However, its performance declined for the VIN class, where it exhibited lower precision coupled with higher recall. Conversely, for the OTH class, the model achieved substantially higher precision than recall. The XGB model alone struggled to recognize VIN and ACT, yet it discriminated OLI relatively well and demonstrated higher recall than precision for the OTH class. The confusion matrix (Supplementary Fig. 7) analysis reveals that the XGB + HB model performs better across various crop types compared to the XGB model alone. However, it exhibits more errors in the OTH class, which is frequently misclassified as one of the other crops. In contrast, the standalone XGB model fails entirely in identifying ACT, often misclassifying it as VIN or OTH. The spatial distribution of misclassifications (Supplementary Fig. 8) highlights a significant border effect for the XGB + HB model, with errors occurring primarily along the field boundaries. In contrast, the standalone XGB model frequently fails to accurately classify entire fields.

4.5. Test area 4

In Test Area 4, the standalone XGB model outperformed the XGB + HB model, with overall accuracies of 0.90 and 0.81, respectively. The XGB model excelled in distinguishing the OTH class, whereas the XGB + HB model struggled more with the background class. The metrics (Table 7) show that the VIN class had a slightly higher F1 score in the XGB + HB model, characterized by high recall but low precision. The opposite pattern was observed in the standalone XGB model, where precision was higher than recall. The confusion matrix (Supplementary Fig. 9) analysis reveals that the XGB model misclassified a substantial portion of VIN as OTH. In contrast, the XGB + HB model performed better in identifying the VIN class, although it resulted in several false positives. Additionally, a small proportion of misclassifications in the XGB + HB model involved incorrectly labeling OTH areas as OLI. The spatial error analysis (Supplementary Fig. 10) indicates that the XGB + HB model misclassification occurs, as previously observed, along the boundary between two classes. However, in this case, there are multiple misclassifications corresponding to different wooded areas or scattered pixels within fields. The standalone XGB model often misclassifies more compact sections, particularly with VIN areas being identified as the OTH class.

4.6. Final classification

The final classification show (Fig. 7, Table 8) the distribution and the extension of the orchards in the AOI.

Olive groves and vineyards are the most widespread, with areas of 1.3 million hectares and 820 thousand hectares, respectively. Olive cultivation exhibits a compact distribution across coastal sectors in central and southern Italy, with significant concentrations in Puglia and Sicily, and fragmented presence along the coastal band. Noteworthy extensions are also observed in the north around Lake Garda. Vineyards, conversely, display dense clusters in Triveneto, Asti, Tuscany, and the westernmost part of Sicily, with substantial extensions along the Adriatic coast. Citrus fruits account for 131 thousand hectares and stone fruits for 150 thousand hectares. Citrus cultivation is primarily located in southern Italy, extending into eastern Sicily, Calabria, and the Metaponto region, while stone fruits are more dispersed, with notable clusters in the Ravenna, Forlì, and Bologna areas, as well as in Campania, northern Puglia, and Metaponto. Pears and apples show strong clustering, with apples concentrated in the Alpine valleys and pears in the central Po Valley, appearing as numerous small-scale orchards. Lastly, actinidia cultivation is heavily clustered in the provinces of Latina, Ravenna, and Cuneo, with approximately 20 thousand hectares classified.

Table 6
Metrics for XGB + HB and XGB models in Test Area 3.

Model	Class	Precision	Recall	F1 Score
XGB + HB	ACT	0.87	0.81	0.84
XGB + HB	OTH	0.88	0.54	0.67
XGB + HB	OLI	0.79	0.94	0.86
XGB + HB	VIN	0.35	0.68	0.47
XGB	ACT	0.92	0.02	0.05
XGB	OTH	0.41	0.62	0.50
XGB	OLI	0.82	0.74	0.78
XGB	VIN	0.05	0.37	0.09

Table 7
Metrics for XGB + HB and XGB models in Test Area 4.

Model	Class	Precision	Recall	F1 Score
XGB + HB	OTH	1.00	0.81	0.89
XGB + HB	VIN	0.29	0.86	0.43
XGB	OTH	0.97	0.93	0.95
XGB	VIN	0.64	0.30	0.40

5. Discussion and conclusion

5.1. Accuracy of the models

This study focused on a method for high-resolution mapping of orchards at a national scale in a heterogeneous context such as Italy. The method involves a pyramid sampling approach of a multi-temporal cube of Sentinel-1 and Sentinel-2 images. The process itself, using a single classifier (XGB) is able to yield appreciable results with high accuracy. However, the incorporation of probabilistic XGB and a Bayesian model based on prior knowledge of regional crop distribution led to improved discrimination of crops, particularly those underrepresented in the dataset due to their lower abundance. The output metrics are consistent with the findings of Campos-Taberner et al. (2020), who adopted a similar classification scheme (CIT, OLI, VIN) and included mixed fruit orchards, leveraging time-series data and LSTM-based algorithms for analysis. Overall, the predictive performance is primarily driven by the XGB model, although the Bayesian framework refines probability distributions, its corrective effect remains limited when the initial XGB predictions are highly polarized. As evidenced in the misclassification maps (Supplementary Figs. 4, 6, 8, 10), in Test 1 large, homogeneous polygons of vineyards and olive groves are classified with high accuracy using XGB alone. This suggests that for classes well represented in the training dataset and in regions characterized by compact land cover, the XGB model effectively captures distinct spectral-temporal patterns, resulting in reliable classification outcomes. However, the dataset is markedly imbalanced, with a strong predominance of OLI, VIN, and OTH, while other crop classes are underrepresented. This imbalance induces systematic misclassifications, particularly along field boundaries, where mixed pixels are preferentially assigned to the dominant classes. The primary challenge thus lies in accurately classifying underrepresented crops. In Test 1, even with the integration of the HB model, no substantial improvement in the F1 score was observed for stone fruits (S.F.), which are both locally scarce and underrepresented in the training set. In this area, where statistical data also indicate a high local prevalence of vineyards and olive groves, the classification of a crop scarcely represented at both the training and territorial levels remains suboptimal. Test 2 further illustrates the limitations of XGB in the absence of territorial constraints, as the model exhibits a strong

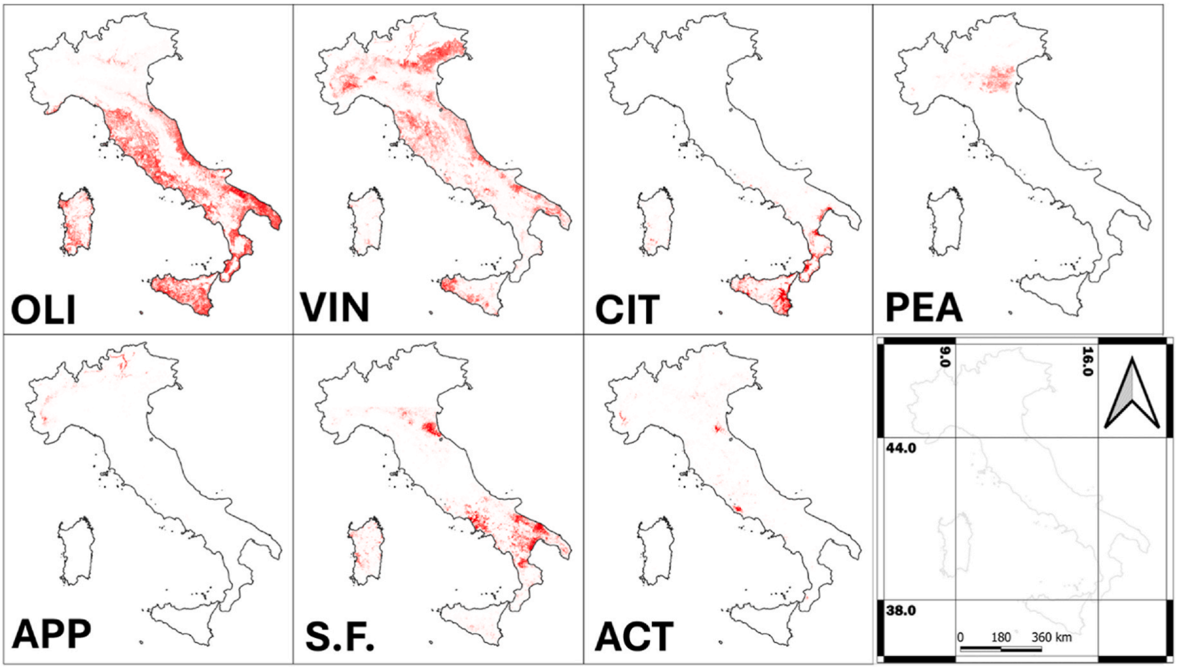

Fig. 7. Final classifications of various land cover classes within the area of interest (AOI).

Table 8
Total areas computed in hectares, with variations analyzed in comparison to statistical reference data.

Class	ha	Difference (%)
ACT	20614	−17
CIT	99876	−16
S.F.	105719	−38
APP	40480	−28
OLI	1773700	58
PEA	20097	−22
VIN	892971	21

tendency to overestimate the vineyard (VIN) class at the expense of apple orchards (APP), which are less represented in the training data, leading to frequent misclassifications of border pixels as VIN or OTH. However, in this province, where local statistics indicate a higher prevalence of apples compared to vineyards, the uncertain pixels that possessed a non-negligible probability of being APP during the Bayesian phase were subsequently reclassified correctly. Test 3 underscores the difficulty of accurately classifying severely underrepresented classes such as actinidia (ACT). Despite its substantial presence within the test area, ACT is predominantly misclassified as OTH or VIN, likely due to the overwhelming representation of these classes in the training data. The integration of HB, however, effectively leverages the weak but non-zero initial ACT probabilities from XGB to reassign pixels more accurately, resulting in a significant improvement in the F1 score for this class. Test 4 reveals a potential drawback of the HB approach in regions characterized by highly polarized crop distributions in the statistical dataset. In areas with a high prevalence of vineyards, XGB already tends to misclassify non-vineyard areas as VIN, likely owing to spectral and phenological similarities of the local vegetation. The Bayesian component further amplifies this misclassification by reinforcing the prior probability distribution, leading to an overestimation of vineyard coverage and an increased false positive rate. This also means that in areas where a particular crop is statistically absent, misclassifications involving less common crops are avoided. Indeed, in Test 4 no misclassifications from background to other crop types were reported, including OLI, which is consistently the most represented class in the training set. In general, the proposed approach demonstrates high accuracy for dominant crops in the training set and those with strong regional prevalence. However, it exhibits limitations in classifying underrepresented orchard classes due to the inherent data imbalance. This constraint affects the detection of minor crops at a national scale and those cultivated outside their typical ecological niche. Conversely, overrepresented classes may be subject to overclassification, particularly in regions where their presence is statistically dominant. The likelihood of identifying a crop in an area where it is absent remains low unless its spectral-temporal signature closely aligns with the training data and is robustly detected by XGB.

5.2. AOI classification

The final analysis (Table 8) provides a comprehensive and reliable overview of the Italian orchard system, highlighting regional trends and crop concentrations (Fig. 7). Vineyards emerge as the most spatially widespread crop, with a significant presence from north to south. Olive cultivation dominates in the central and southern regions, particularly in Puglia, while citrus (CIT) is primarily concentrated in the southernmost areas, with extensive coverage in eastern Sicily, Calabria, and Metaponto. Stone fruits show a more fragmented distribution, concentrated in specific districts such as the coastal areas of Emilia-Romagna, Campania, and Puglia. Apples (APP) are predominantly found in the alpine valleys of Trentino and South Tyrol, with some presence in the Cuneo province. Pears (PEA) are strongly concentrated in the central Po plain, particularly around Ferrara, while ACT are cultivated almost exclusively in Latina, Cuneo, and Emilia-Romagna.

From a quantitative perspective, some limitations of pixel-based classification must be considered. As noted in previous studies (Carfagna and Gallego, 2005), summing pixel data to determine the actual crop extent can introduce biases. In this case a significant issue is the misclassification of certain crops, particularly olives and vineyards, which dominate national agricultural statistics and the training dataset. This leads to an overestimation of these crops, with olive groves overestimated by 58 % and vineyards by 21 %. Olive groves present specific challenges due to their irregular planting patterns, with trees often widely spaced and scattered over large areas. Moreover, olive trees are frequently found in mixed environments, such as polyculture systems or private gardens, complicating their classification further. This issue of irregular olive grove layouts has been highlighted by other authors, who report challenges in extracting specific textures even at high resolution. Despite this, overall accuracy (OA) values of up to 0.94 have been achieved for olive detection in specific test areas (Lin et al., 2021). Vineyards class had misclassifications involving green areas that share similar phenology, particularly in regions with high concentrations of vineyards. Other studies support a higher recall in vineyard detection, indicating that non-vineyard areas are more frequently misclassified as vineyards when using medium-resolution satellite images (López et al., 2008; Campos-Taberner et al., 2020). The other crops were generally underestimated, with the largest discrepancy noted for stone fruits, which were underestimated by 38 %. Citrus crops were slightly underestimated by 16 %, while pears, apples, and actinidia were underestimated by 22 %, 26 %, and 17 %, respectively. These crops are typically distributed across all provinces, yet they occur in very low concentrations. As a result, the Bayesian approach may struggle to accurately capture their overall presence, particularly in regions where their occurrence is minimal. Accuracy tends to be higher in major growing areas, however, this is contingent upon the confidence levels of the XGB model. Therefore, the predominant source of misclassification in these classes can be attributed to the limited predictive capability of the XGB model. This issue is to be expected, as the scarcity of training samples leads to underrepresented classes, which inherently exhibit lower classification accuracies (Valero et al., 2021; Chabalala et al., 2023). This is especially evident in scenarios where the classes encompass multiple crop types and various plastic-covered surfaces (Castellano et al., 2008) over a large and heterogeneous area (Defourny et al., 2019, Pelletier et al., 2016). As observed in the Supplementary Material, a significant portion of misclassifications arises from an edge effect, where XGB misclassifies minor crops as dominant ones, primarily olive groves and vineyards. This effect must not be overlooked, as it may introduce a substantial surface-area bias (Li et al., 2023; Gallego, 2004).

5.3. Limitation and future perspectives

Despite achieving high classification accuracy, this study exhibits inherent limitations. The methodology relies on ground sampling and statistical datasets, which may be incomplete or inconsistent across regions and nation, potentially affecting approach performance and generalizability. The classifier demonstrates optimal performance in regions where crops are well-established due to extensive data availability but encounters limitations in non-traditional cultivation areas due to sparse observations and temporal-spectral variability driven by differing management practices and phenological cycles. While the primary focus remains on major crop regions, secondary cultivation areas warrant further investigation (Weikmann et al., 2021). Nevertheless, transferability the models could be viable in agroecologically analogous regions (e.g., Mediterranean zones), extending beyond national boundaries. The statistical model facilitates the detection of underrepresented crops while maintaining low computational costs, however, its efficacy is maximized in highly polarized agricultural landscapes, such as Italy. In homogeneous agricultural systems characterized by low variability, its applicability may be constrained. A substantial proportion of classification errors originates from edge effects, particularly at field boundaries. This issue is inherently linked to sensor resolution and can be exacerbated in highly fragmented agricultural landscapes. The integration of object-based classification methods or convolutional neural networks (CNNs) could mitigate these inaccuracies by refining field delineation and incorporating prior spatial information into the classification process (Lu et al., 2024; Song et al., 2023). Methodological enhancements could involve the implementation of data augmentation strategies to improve class balance (Sharma and Gosain, 2025) and the refinement of the area of interest (AOI) definition, reducing background classification noise. This could be achieved by integrating supplementary LULC layers, which can provide high-resolution and context information on settlements or forested areas (Karra et al., 2021; Yu et al., 2018). Furthermore, spectral indices could be leveraged to pre-classify orchard and non-orchard areas (Chen et al., 2024), facilitating the generation of a targeted mask that isolates fruit cultivation zones (Valero et al., 2016). The adoption of such approaches could enhance classification accuracy and overall model robustness.

5.4. Conclusion

This study presents a nationwide 10-m resolution mapping of Italy's major woody crops. By delineating the agricultural domain using CORINE Land Cover and implementing a pyramidal sampling strategy for key orchard classes, a Sentinel-1 and Sentinel-2 spectro-temporal data cube was leveraged to generate a high-resolution crop distribution layer, currently unavailable at this scale and detail. An XGB classifier was implemented, leveraging a probabilistic output rather than a deterministic class assignment, thereby enabling a soft classification approach. While the XGB model achieved high overall accuracy, it exhibited limitations in predicting underrepresented crops due to dataset imbalance. To further refine class probabilities, a hierarchical Bayesian model was integrated, incorporating national crop coverage statistics as priors. This approach improved the representation of minor crops by leveraging prior knowledge, mitigating the constraints of traditional hard classification. While this Bayesian framework enhanced minor crop detection, it introduced a trade-off, particularly in regions dominated by major crops at the national scale. In boundary and marginal areas, the model tended to overestimate primary classes, increasing false positives.

The resulting dataset establishes a foundation for large-scale, cycle-based agricultural monitoring using freely available satellite imagery. Future advancements may further refine this approach, enhancing its applicability in precision agriculture and policy development.

CRediT authorship contribution statement

Francesco Lodato: Writing – review & editing, Writing – original draft, Methodology, Data curation, Conceptualization. **Ryan Jayne:** Writing – review & editing, Software, Methodology, Data curation. **Marco Santonico:** Writing – review & editing, Validation, Supervision. **Maurizio Pollino:** Writing – review & editing, Validation, Methodology. **Flavio Bellino:** Writing – review & editing, Validation. **Laura De Gara:** Writing – review & editing, Validation, Supervision. **Bruno Basso:** Writing – review & editing, Supervision, Resources, Project administration, Funding acquisition, Conceptualization.

Data

The final classification of the AOI, refined through sieving at 10 pixel threshold, will be publicly available.

Declaration of competing interest

The authors declare the following financial interests/personal relationships which may be considered as potential competing interests.

Acknowledgements

The authors wish to express their gratitude to the staff of TIMAC AGRO Italia for their assistance in data acquisition and for funding the PhD scholarship for the 37th cycle in AI Agrifood. Special thanks also to Brian Baer for his IT support. Partial funding is provided to Basso by the USDA-NIFA AIFARMS project Award No, 2020-67021-32799; Michigan State University AgBioResearch. Partial funding to Basso is provided by USDA-NIFA AIFARM project Award No. 2020-67021-32799, and Michigan State University AgBioResearch.

Appendix A. Supplementary data

Supplementary data to this article can be found online at https://doi.org/10.1016/j.srs.2025.100237.

Data availability

Data will be made available on request.

References

Abozeid, A., Alanazi, R., Elhadad, A., Taloba, A.I., Abd El-Aziz, R.M., 2022. A large-scale dataset and deep learning model for detecting and counting olive trees in satellite imagery. Comput. Intell. Neurosci. 2022 (1), 1549842.

Abubakar, M.A., Chanzy, A., Flamain, F., Pouget, G., Courault, D., 2023. Delineation of orchard, vineyard, and Olive trees based on phenology metrics derived from time series of Sentinel-2. Remote Sens. 15 (9), 2420.

Ahmed, S.A., N, H., 2023. Land use and land cover classification using machine learning algorithms in google earth engine. Earth Science Informatics 16 (4), 3057–3073.

Arfah, S., Sencaki, D.B., Permata, Z.D.O., Putri, M.N., Sanjaya, H., 2021. Land cover change in badung regency 2016-2020: an approach using machine learning method: random forest & extreme gradient boost (XGB). In: 2021 IEEE Asia-Pacific Conference on Geoscience, Electronics and Remote Sensing Technology (AGERS). IEEE, pp. 38–45.

Bartolini, G., Petruccelli, R., 2002. Classification, Origin, Diffusion and History of the Olive. Food & Agriculture Org.

Bhagwat, R.U., Shankar, B.U., 2019. A novel multilabel classification of remote sensing images using XGBoost. In: 2019 IEEE 5th International Conference for Convergence in Technology (I2CT). IEEE, pp. 1–5.

Blei, D.M., Kucukelbir, A., McAuliffe, J.D., 2017. Variational inference: a review for statisticians. J. Am. Stat. Assoc. 112 (518), 859–877.

Boryan, C., Yang, Z., Mueller, R., Craig, M., 2011. Monitoring US agriculture: the US department of agriculture, national agricultural statistics service, cropland data layer program. Geocarto Int. 26 (5), 341–358.

Bouguettaya, A., Zarzour, H., Kechida, A., Taberkit, A.M., 2022. Deep learning techniques to classify agricultural crops through UAV imagery: a review. Neural Comput. Appl. 34 (12), 9511–9536.

Büttner, G., Feranec, J., Jaffrain, G., Mari, L., Maucha, G., Soukup, T., 2004. The CORINE land cover 2000 project. EARSeL eProceedings 3 (3), 331–346.

Campos-Taberner, M., García-Haro, F.J., Martínez, B., Izquierdo-Verdiguier, E., Atzberger, C., Camps-Valls, G., Gilabert, M.A., 2020. Understanding deep learning in land use classification based on Sentinel-2 time series. Sci. Rep. 10 (1), 17188.

Carfagna, E., Gallego, F.J., 2005. Using remote sensing for agricultural statistics. Int. Stat. Rev. 73 (3), 389–404.

Carrasco, L., O'Neil, A.W., Morton, R.D., Rowland, C.S., 2019. Evaluating combinations of temporally aggregated sentinel-1, sentinel-2 and landsat 8 for land cover mapping with google earth engine. Remote Sens. 11 (3), 288.

Castellano, S., Mugnozza, G.S., Russo, G., Briassoulis, D., Mistrotis, A., Hemming, S., Waaijenberg, D., 2008. Design and use criteria of netting systems for agricultural production in Italy. J. Agric. Eng. 39 (3), 31–42.

Chabalala, Y., Adam, E., Ali, K.A., 2023. Exploring the effect of balanced and imbalanced multi-class distribution data and sampling techniques on fruit-tree crop classification using different machine learning classifiers. Geomatics 3 (1), 70–92.

Chen, T., Guestrin, C., 2016. Xgboost: a scalable tree boosting system. In: Proceedings of the 22nd Acm Sigkdd International Conference on Knowledge Discovery and Data Mining, pp. 785–794.

Chen, Y., Lu, D., Moran, E., Batistella, M., Dutra, L.V., Sanches, I.D.A., et al., 2018. Mapping croplands, cropping patterns, and crop types using MODIS time-series data. Int. J. Appl. Earth Obs. Geoinf. 69, 133–147.

Chen, R., Yang, H., Liu, W., Liu, M., Qi, N., Feng, H., et al., 2024. An orchard mapping index and mapping algorithm coupling orchard phenology and green-holding characteristics from time-series sentinel-2 images. Comput. Electron. Agric. 226, 109437.

Cogato, A., Pezzuolo, A., Sozzi, M., Marinello, F., 2020. A sample of Italian vineyards: landscape and management parameters dataset. Data Brief 33, 106589.

Corsi, A., Mazzarino, S., Pomarici, E., 2019. The Italian Wine Industry. The Palgrave handbook of wine industry economics, pp. 47–76.

Costantini, E.A., Barbetti, R., 2008. Environmental and visual impact analysis of viticulture and olive tree cultivation in the province of Siena (Italy). Eur. J. Agron. 28 (3), 412–426.

Dal Ferro, N., Borin, M., 2017. Environment, agro-system and quality of food production in Italy. Ital. J. Agron. 12 (2), 793.

Defourny, P., Bontemps, S., Bellemans, N., Cara, C., Dedieu, G., Guzzonato, E., et al., 2019. Near real-time agriculture monitoring at national scale at parcel resolution: performance assessment of the Sen2-Agri automated system in various cropping systems around the world. Rem. Sens. Environ. 221, 551–568.

d'Andrimont, R., Verhegghen, A., Lemoine, G., Kempeneers, P., Meroni, M., Van Der Velde, M., 2021. From parcel to continental scale–A first European crop type map based on Sentinel-1 and LUCAS Copernicus in-situ observations. Rem. Sens. Environ. 266, 112708.

ESA, 2023a. Sentinel-1. sentinel.esa.int/web/sentinel/missions/sentinel-1. https://sentinel.esa.int/web/sentinel/missions/sentinel-1. (Accessed 27 October 2023).

ESA, 2023b. Sentinel-2. sentinel.esa.int/web/sentinel/missions/sentinel-2. https://sentinel.esa.int/web/sentinel/missions/sentinel-2. (Accessed 27 October 2023).

Fan, J., Zhang, X., Zhao, C., Qin, Z., De Vroey, M., Defourny, P., 2021. Evaluation of crop type classification with different high resolution satellite data sources. Remote Sens. 13 (5), 911.

Floreano, I.X., de Moraes, L.A.F., 2021. Land use/land cover (LULC) analysis (2009–2019) with google earth engine and 2030 prediction using markov-CA in the rondônia state, Brazil. Environ. Monit. Assess. 193 (4), 239.

Friedman, J.H., 2001. Greedy function approximation: a gradient boosting machine. Ann. Stat. 1189–1232.

Gallego, F.J., 2004. Remote sensing and land cover area estimation. Int. J. Rem. Sens. 25 (15), 3019–3047.

Gorelick, N., Hancher, M., Dixon, M., Ilyushchenko, S., Thau, D., Moore, R., 2017. Google earth engine: planetary-scale geospatial analysis for everyone. Rem. Sens. Environ. 202, 18–27.

Hütt, C., Koppe, W., Miao, Y., Bareth, G., 2016. Best accuracy land use/land cover (LULC) classification to derive crop types using multitemporal, multisensor, and multi-polarization SAR satellite images. Remote Sens. 8 (8), 684.

Inglada, J., Vincent, A., Arias, M., Marais-Sicre, C., 2016. Improved early crop type identification by joint use of high temporal resolution SAR and optical image time series. Remote Sens. 8 (5), 362.

Ioannidou, M., Koukos, A., Sitokonstantinou, V., Papoutsis, I., Kontoes, C., 2022. Assessing the added value of Sentinel-1 PolSAR data for crop classification. Remote Sens. 14 (22), 5739.

Ioannidou, S.C., Litskas, V.D., Stavrinides, M.C., Vogiatzakis, I.N., 2022. Linking management practices and soil properties to Ecosystem Services in Mediterranean mixed orchards. Ecosyst. Serv. 53, 101378.

Istat, 2022. Coltivazioni superfici e produzione. URL: @online{istat2022, author={Istat},title={{Coltivazioni}Superficieproduzione},year= 2022. http://dati.istat.it/Index.aspx?QueryId=37850. (Accessed 15 October 2023).

Jiang, Y., Lu, Z., Li, S., Lei, Y., Chu, Q., Yin, X., Chen, F., 2020. Large-scale and high-resolution crop mapping in China using Sentinel-2 satellite imagery. Agriculture 10 (10), 433.

Karra, K., Kontgis, C., Statman-Weil, Z., Mazzariello, J.C., Mathis, M., Brumby, S.P., 2021. Global land use/land cover with Sentinel 2 and deep learning. In: 2021 IEEE International Geoscience and Remote Sensing Symposium IGARSS. IEEE, pp. 4704–4707.

Kumar, S., Meena, R.S., Sheoran, S., Jangir, C.K., Jhariya, M.K., Banerjee, A., Raj, A., 2022. Remote sensing for agriculture and resource management. In: Natural Resources Conservation and Advances for Sustainability. Elsevier, pp. 91–135.

Lark, T.J., Schelly, I.H., Gibbs, H.K., 2021. Accuracy, bias, and improvements in mapping crops and cropland across the United States using the USDA Cropland Data Layer. Remote Sens. 13 (5), 968.

Larsen, A.E., Hendrickson, B.T., Dedeic, N., MacDonald, A.J., 2015. Taken as a given: evaluating the accuracy of remotely sensed crop data in the USA. Agric. Syst. 141, 121–125.

Li, H., Song, X.P., Hansen, M.C., Becker-Reshef, I., Adusei, B., Pickering, J., et al., 2023. Development of a 10-m resolution maize and soybean map over China: matching satellite-based crop classification with sample-based area estimation. Rem. Sens. Environ. 294, 113623.

Lin, C., Jin, Z., Mulla, D., Ghosh, R., Guan, K., Kumar, V., Cai, Y., 2021. Toward large-scale mapping of tree crops with high-resolution satellite imagery and deep learning algorithms: a case study of olive orchards in Morocco. Remote Sens. 13 (9), 1740.

Lin, L., Di, L., Zhang, C., Guo, L., Di, Y., Li, H., Yang, A., 2022. Validation and refinement of cropland data layer using a spatial-temporal decision tree algorithm. Sci. Data 9 (1), 63.

Lodato, F., Pennazza, G., Santonico, M., Vollero, L., Grasso, S., Pollino, M., 2024. In-depth analysis and characterization of a hazelnut agro-industrial context through the integration of multi-source satellite data: a case study in the province of viterbo, Italy. Remote Sens. 16 (7), 1227.

López, C.Á., Barros, D.M., Álvarez, M.F., 2008. Vineyard area estimation using medium spatial resolution satellite imagery. Spanish J. Agric. Res. 6 (3), 441–452.

Łoś, H., Mendes, G.S., Cordeiro, D., Grosso, N., Costa, H., Benevides, P., Caetano, M., 2021. Evaluation of XGBoost and LGBM performance in tree species classification with sentinel-2 data. In: 2021 IEEE International Geoscience and Remote Sensing Symposium IGARSS. IEEE, pp. 5803–5806.

Lu, R., Zhang, Y., Huang, Q., Zeng, P., Shi, Z., Ye, S., 2024. A refined edge-aware convolutional neural networks for agricultural parcel delineation. Int. J. Appl. Earth Obs. Geoinf. 133, 104084.

Mahlayeye, M., Darvishzadeh, R., Nelson, A., 2022. Tree-fruits crop type mapping from Sentinel-1 and Sentinel-2 data integration in Egypt's New Delta project, 2022 Remote Sens. Appl.: Society and Environment 27, 100776.

Maleki, R., Wu, F., Oubara, A., Fathollahi, L., Yang, G., 2024. Refinement of cropland data layer with effective confidence layer interval and image filtering. Agriculture 14 (8), 1285.

Nabil, M., Farg, E., Arafat, S.M., Aboelghar, M., Afify, N.M., Elsharkawy, M.M., 2022. Tree-fruits crop type mapping from sentinel-1 and sentinel-2 data integration in Egypt's new delta project. Remote Sensing Applications: Society and Environment 27, 100776.

Ng, A., Jordan, M., 2001. On discriminative vs. generative classifiers: a comparison of logistic regression and naive bayes. Adv. Neural Inf. Process. Syst. 14.

Nigar, A., Li, Y., Jat Baloch, M.Y., Alrefaei, A.F., Almutairi, M.H., 2024. Comparison of machine and deep learning algorithms using Google Earth Engine and Python for land classifications. Front. Environ. Sci. 12, 1378443.

Orynbaikyzy, A., Gessner, U., Mack, B., Conrad, C., 2020. Crop type classification using fusion of sentinel-1 and sentinel-2 data: assessing the impact of feature selection,

optical data availability, and parcel sizes on the accuracies. Remote Sens. 12 (17), 2779.
Özlem, A., Saralioğlu, E., Güngör, O., Bayata, H.F., 2024. Semantic segmentation of very-high spatial resolution satellite images: A comparative analysis of 3d CNN and traditional machine learning algorithms for automatic vineyard detection. International Journal of Engineering and Geosciences 9, 12–24.
Pasha, S.V., Dadhwal, V.K., Saketh, K., 2023. Remote sensing for mango and rubber mapping and characterization for carbon stock estimation—case Study of Malihabad Tehsil (UP) and West Tripura District, India. In: Digital Ecosystem for Innovation in Agriculture. Springer Nature Singapore, Singapore, pp. 183–200.
Pelletier, C., Valero, S., Inglada, J., Champion, N., Dedieu, G., 2016. Assessing the robustness of Random Forests to map land cover with high resolution satellite image time series over large areas. Rem. Sens. Environ. 187, 156–168.
Peng, Y., Qiu, B., Tang, Z., Xu, W., Yang, P., Wu, W., et al., 2024. Where is tea grown in the world: a robust mapping framework for agroforestry crop with knowledge graph and sentinels images. Rem. Sens. Environ. 303, 114016.
Pluto-Kossakowska, J., 2021. Review on multitemporal classification methods of satellite images for crop and arable land recognition. Agriculture 11 (10), 999.
Prins, A.J., Van Niekerk, A., 2021. Crop type mapping using LiDAR, Sentinel-2 and aerial imagery with machine learning algorithms. Geo Spatial Inf. Sci. 24 (2), 215–227.
Roy, S., More, R., Kimothi, M.M., Mamatha, S., Vyas, S.P., Ray, S.S., 2018. Comparative analysis of object based and pixel based classification for mapping of mango orchards in Sitapur district of Uttar Pradesh. J Geomatics 12 (1), 1–8.
Sahu, H., Haldar, D., Danodia, A., Kumar, S., 2018. Classification of orchard crop using sentinel-1A synthetic aperture radar data. Int. Arch. Photogram. Rem. Sens. Spatial Inf. Sci. 42, 335–338.
Saini, R., Ghosh, S.K., 2021. Crop classification in a heterogeneous agricultural environment using ensemble classifiers and single-date Sentinel-2A imagery. Geocarto Int. 36 (19), 2141–2159.
Sasso, D., Lodato, F., Sabatini, A., Pennazza, G., Vollero, L., Santonico, M., Merone, M., 2024. Hazelnut mapping detection system using optical and radar remote sensing: benchmarking machine learning algorithms. Artificial Intelligence in Agriculture 12, 97–108.
Shafizadeh-Moghadam, H., Khazaei, M., Alavipanah, S.K., Weng, Q., 2021. Google Earth Engine for large-scale land use and land cover mapping: an object-based classification approach using spectral, textural and topographical factors. GIScience Remote Sens. 58 (6), 914–928.
Shao, Z., Ahmad, M.N., Javed, A., 2024. Comparison of random forest and xgboost classifiers using integrated optical and sar features for mapping urban impervious surface. Remote Sens. 16 (4), 665.
Sharma, S., Gosain, A., 2025. Addressing class imbalance in remote sensing using deep learning approaches: a systematic literature review. Evolutionary Intelligence 18 (1), 1–28.
Shelestov, A., Lavreniuk, M., Kussul, N., Novikov, A., Skakun, S., 2017. Large scale crop classification using Google earth engine platform. In: 2017 IEEE International Geoscience and Remote Sensing Symposium (IGARSS). IEEE, pp. 3696–3699.
Song, X.P., Huang, W., Hansen, M.C., Potapov, P., 2021. An evaluation of Landsat, Sentinel-2, Sentinel-1 and MODIS data for crop type mapping. Science of Remote Sensing 3, 100018.
Song, W., Wang, C., Dong, T., Wang, Z., Wang, C., Mu, X., Zhang, H., 2023. Hierarchical extraction of cropland boundaries using Sentinel-2 time-series data in fragmented agricultural landscapes. Comput. Electron. Agric. 212, 108097.
Stillitano, T., De Luca, A.I., Falcone, G., Spada, E., Gulisano, G., Strano, A., 2016. Economic profitability assessment of Mediterranean olive growing systems. Bulgarian Journal of Agricultural Science 22 (4).
Stillitano, T., De Luca, A.I., Iofrida, N., Falcone, G., Spada, E., Gulisano, G., 2017. Economic analysis of olive oil production systems in southern Italy. Calitatea 18 (157), 107.
Sun, L., Chen, J., Guo, S., Deng, X., Han, Y., 2020. Integration of time series sentinel-1 and sentinel-2 imagery for crop type mapping over oasis agricultural areas. Remote Sens. 12 (1), 158.
Sweidan, D., Johansson, U., 2021. Probabilistic prediction in scikit-learn. In: The 18th International Conference on Modeling Decisions for Artificial Intelligence, On-Line (From Umeå, Sweden). September 27-30, 2021.
Tassi, A., Vizzari, M., 2020. Object-oriented lulc classification in google earth engine combining snic, glcm, and machine learning algorithms. Remote Sens. 12 (22), 3776.
Teluguntla, P., Thenkabail, P.S., Xiong, J., Gumma, M.K., Giri, C., Milesi, C., et al., 2015. Global Food Security Support Analysis Data (GFSAD) at Nominal 1 Km (GCAD) Derived from Remote Sensing in Support of Food Security in the Twenty-First Century: Current Achievements and Future Possibilities.
Toosi, A., Javan, F.D., Samadzadegan, F., Mehravar, S., Kurban, A., Azadi, H., 2022. Citrus orchard mapping in Juybar, Iran: analysis of NDVI time series and feature fusion of multi-source satellite imageries. Ecol. Inform. 70, 101733.
Torquati, B., Giacchè, G., Venanzi, S., 2015. Economic analysis of the traditional cultural vineyard landscapes in Italy. J. Rural Stud. 39, 122–132.
Tubiello, F.N., Conchedda, G., Casse, L., Pengyu, H., Zhongxin, C., De Santis, G., et al., 2023. Measuring the world's cropland area. Nat. Food 4 (1), 30–32.
Valero, S., Morin, D., Inglada, J., Sepulcre, G., Arias, M., Hagolle, O., et al., 2016. Production of a dynamic cropland mask by processing remote sensing image series at high temporal and spatial resolutions. Remote Sens. 8 (1), 55.
Valero, S., Arnaud, L., Planells, M., Ceschia, E., 2021. Synergy of Sentinel-1 and Sentinel-2 imagery for early seasonal agricultural crop mapping. Remote Sens. 13 (23), 4891.
Wang, Y., Sun, Y., Cao, X., Wang, Y., Zhang, W., Cheng, X., 2023. A review of regional and Global scale Land Use/Land Cover (LULC) mapping products generated from satellite remote sensing. ISPRS J. Photogrammetry Remote Sens. 206, 311–334.
Wardlow, B.D., Egbert, S.L., 2008. Large-area crop mapping using time-series MODIS 250 m NDVI data: an assessment for the US Central Great Plains. Rem. Sens. Environ. 112 (3), 1096–1116.
Wardlow, B.D., Egbert, S.L., Kastens, J.H., 2007. Analysis of time-series MODIS 250 m vegetation index data for crop classification in the US Central Great Plains. Rem. Sens. Environ. 108 (3), 290–310.
Weikmann, G., Paris, C., Bruzzone, L., 2021. Timesen2crop: a million labeled samples dataset of sentinel 2 image time series for crop-type classification. IEEE J. Sel. Top. Appl. Earth Obs. Rem. Sens. 14, 4699–4708.
Weissteiner, C.J., Strobl, P., Sommer, S., 2011. Assessment of status and trends of olive farming intensity in EU-Mediterranean countries using remote sensing time series and land cover data. Ecol. Indic. 11 (2), 601–610.
Xue, J., Zhang, X., Chen, S., Hu, B., Wang, N., Shi, Z., 2024. Quantifying the agreement and accuracy characteristics of four satellite-based LULC products for cropland classification in China. J. Integr. Agric. 23 (1), 283–297.
Yao, J., Wu, J., Xiao, C., Zhang, Z., Li, J., 2022. The classification method study of crops remote sensing with deep learning, machine learning, and Google Earth engine. Remote Sens. 14 (12), 2758.
Yu, L., Su, J., Li, C., Wang, L., Luo, Z., Yan, B., 2018. Improvement of moderate resolution land use and land cover classification by introducing adjacent region features. Remote Sens. 10 (3), 414.
Zhang, C., Marzougui, A., Sankaran, S., 2020. High-resolution satellite imagery applications in crop phenotyping: an overview. Comput. Electron. Agric. 175, 105584.
Zhang, H., Kang, J., Xu, X., Zhang, L., 2020. Accessing the temporal and spectral features in crop type mapping using multi-temporal Sentinel-2 imagery: a case study of Yi'an County, Heilongjiang province, China. Comput. Electron. Agric. 176, 105618.
Zhang, T., Hu, D., Wu, C., Liu, Y., Yang, J., Tang, K., 2023. Large-scale apple orchard mapping from multi-source data using the semantic segmentation model with image-to-image translation and transfer learning. Comput. Electron. Agric. 213, 108204.
Zhao, Z., Islam, F., Waseem, L.A., Tariq, A., Nawaz, M., Islam, I.U., et al., 2024. Comparison of three machine learning algorithms using google earth engine for land use land cover classification. Rangel. Ecol. Manag. 92, 129–137.
Zhou, G., Ni, Z., Zhao, Y., Luan, J., 2022. Identification of bamboo species based on Extreme Gradient Boosting (XGBoost) using Zhuhai-1 orbita hyperspectral remote sensing imagery. Sensors (Peterb., NH) 22 (14), 5434.